Supplementary Information

Astaxanthin targets IL-6 and alleviates the LPS-induced adverse inflammatory response of macrophages

Yahui Wu [a,b], Mona A. Bashir [a,b], Changsheng Shao [c], Han Wang [a,b], Jianxia Zhu [a,d], Qing Huang [a,b,*]

[a] *CAS Key Laboratory of High Magnetic Field and Ion Beam Physical Biology, Anhui Key Laboratory of Environmental Toxicology and Pollution Control Technology, Hefei Institute of Intelligent Agriculture, Institute of Intelligent Machines, Hefei Institutes of Physical Science, Chinese Academy of Sciences, Hefei 230031, China.*

[b] *Science Island Branch of Graduate School, University of Science & Technology of China, Hefei 230026, China.*

[c] *High Magnetic Field Laboratory, Hefei Institutes of Physical Science, Chinese Academy of Sciences, Hefei 230031, China.*

[d] *School of Nursing, Anhui Medical University, Hefei, Anhui 230032, China.*

* Corresponding author: Professor Qing Huang

Tel: 86-551-65595261; Fax: 86-551-65595261

Email: huangq@ipp.ac.cn

ORCID: 0000-0002-8884-2064

24 **The supplementary information contains the following parts:**

25 Fig. S1 PMA induced THP-1 monocytes to differentiate into macrophages.

26 Fig. S2 Effect of different concentrations of LPS and AST on the viability of THP-1-derived

27 macrophages.

28 Fig. S3 AST targets and inflammatory targets.

29 Fig. S4 Molecular docking analysis and molecular dynamics simulation of AST-TNF-α.

30 Fig. S5 The expression of TNF-α, STAT3 and NF-κB mRNA levels after the interference of TNF-

31 α siRNA

32 Table S1 PCR primer sequences.

33 Table S2 Partial core target attributes.

34 Table S3 Binding energy of IL-6 and AST.

We initially induced THP-1 cells with 100 ng/mL PMA for 24 h to prompt differentiation into macrophages. Morphological observations were recorded, including images. Morphological observations revealed that untreated cells were transparent and spherical, remaining suspended after 24 h of culture. Following induction with 100 ng/mL PMA for 24 h, cells exhibited irregular shapes, a fusiform morphology, with protruding pseudopods and adherent growth. Flow cytometry was also employed to measure the expression level of the THP-1-derived macrophage-specific protein CD11b. Flow cytometry results indicated a significant increase in the expression of the cell surface-specific protein CD11b after induction with 100 ng/mL PMA, suggesting the successful differentiation of THP-1 monocytes into macrophages (Fig. S1A-B).

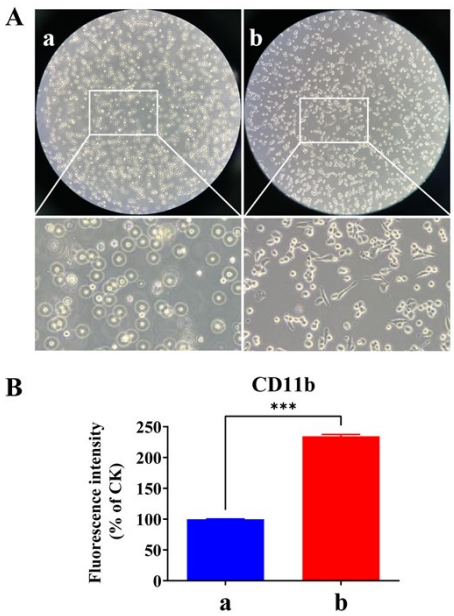

Fig. S1 PMA induced THP-1 monocytes to differentiate into macrophages. (A) Cell morphology observation (×40). (B) Expression of cell surface specific protein CD11b. a: uninduced group; b:100 ng/mL PMA induction group. (n = 3/group; mean ± SD; *** represent $p < 0.001$.)

We assessed the cytotoxic effect of LPS on THP-1 macrophages using a CCK-8 assay. Under our experimental conditions, no significant change in cell viability was observed at a mass concentration of 1.0 μg/mL ($p > 0.05$). However, other concentrations of LPS demonstrated varying degrees of inhibition on THP-1 cell viability. Therefore, we selected LPS with a concentration of 1.0 μg/mL as the optimal treatment concentration for the experiment (Fig. S2A).

The optimal treatment concentration of AST was screened under the concentration of LPS. Different concentration gradients of AST (0, 25, 50, 100 μM) were used to treat the cells for 3 h, and then the screened LPS concentration (1.0 μg/mL) was used to stimulate THP-1-derived macrophages to produce inflammation, and THP-1-derived macrophage viability was determined by CCK-8 assay. The results are shown in the Fig. S2B. With the increase of the concentration, the cell viability showed a general trend of increasing and then decreasing; compared with the 0 μM AST group, the cell viability could be significantly enhanced when the concentration was at 25 μM and 50 μM, and the cell viability was the strongest at the concentration of 50 μM; there was no significant change in cell viability at the concentration of 100 μM. Therefore, AST at 50 μM was selected as the optimal treatment concentration for the experiment.

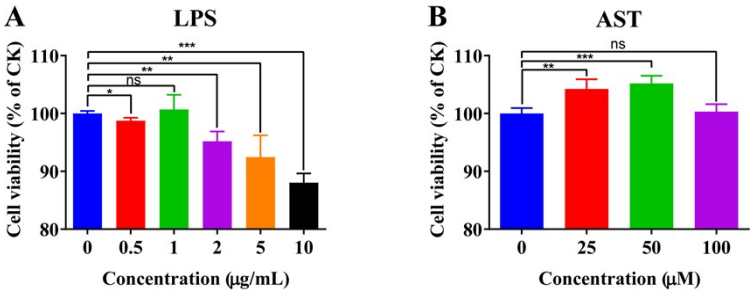

Fig. S2 Effect of different concentrations of LPS and AST on the viability of THP-1-derived macrophages. (A) The effects of different concentrations of LPS on the viability of THP-1-derived macrophages. (B) The effects of different concentrations of AST on the viability of THP-1-derived macrophages. (n = 3/group; mean ± SD; * represent $p < 0.05$; **

represent $p < 0.01$; *** represent $p < 0.001$; ns represent no significant difference compared with the control group.)

The 2D structure of AST was obtained from the Pubchem database, and the AST SMILE name was entered into the SWISS Target Prediction database to obtain 100 potential targets of AST. Using "Inflammation" as the keyword, we searched for targets in GeneCards and DisGeNET databases. 467 inflammation-associated genes were retrieved from DisGeNET database, and 1500 inflammation-associated genes were retrieved and screened from GeneCards database, which gave us a total of 1625 potential disease-activating targets by integrating all the targets and removing duplicates.

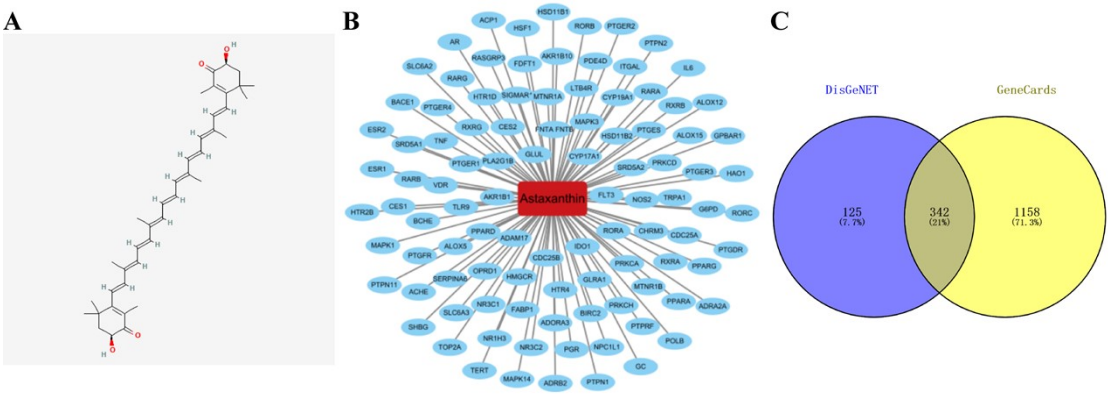

Fig. S3 AST targets and inflammatory targets. (A) Astaxanthin 2D structural diagram. (B) AST-target network diagram. (C) The cross-Venn diagram of inflammatory targets was searched in the database.

To verify whether TNF-α is the target of AST, we used *in silico* calculations based on molecular docking, molecular dynamics simulation, and identified TNF-α also as a target of AST (Fig.S4).

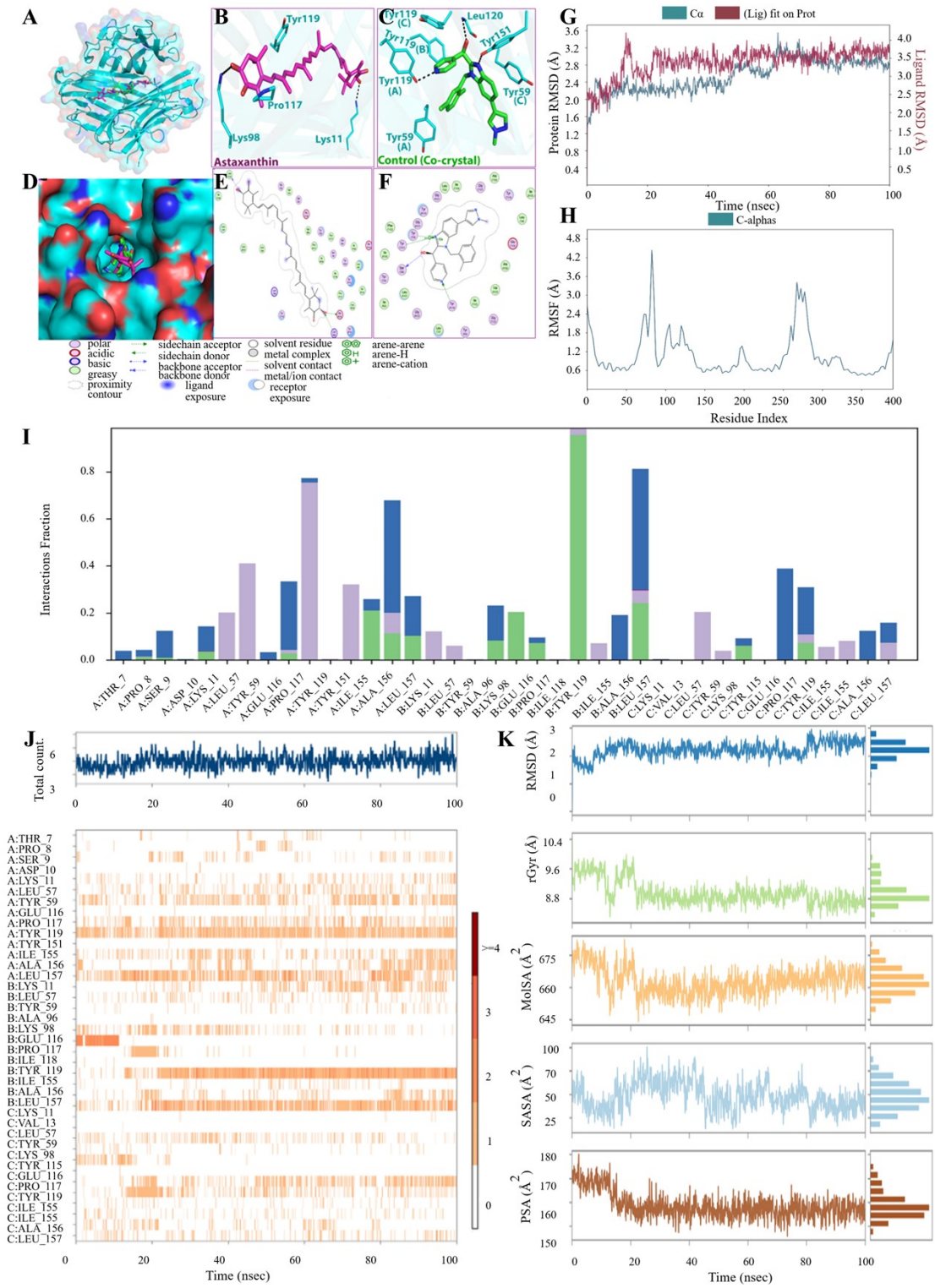

Fig. S4 Molecular docking analysis and molecular dynamics simulation. (A) - (F) 2D and 3D visualization of AST-TNF-α complex. (G) - (H) RMSD (Left) and RMSF (Right) of AST-TNF-α interaction. (I) AST-TNF-α contact mapping shows the hydrogen bonding during 100 ns simulation time. (J) - (K) AST-TNF-α contact mapping shows many amino

acids participate in the interaction of AST with TNF-α (Left) and the behavior of AST inside the TNF-α pocket during 100 ns simulation time (Right).

Furthermore, we conducted the TNF-α interference experiment for comparison. Fig. S5A shows that compared to the LPS (NC) group, the expression of TNF-α in the AST + LPS (NC) group significantly decreased, demonstrating that AST could inhibit the expression of TNF-α. The TNF-α in the LPS (si-TNF-α) group also significantly decreased, confirming the success of the interference experiment. To check whether there is correlation between TNF-α and NF-κB and STAT3, we also examined the expression levels of NF-κB and STAT3 in macrophages after TNF-α interference. As presented in Fig. S5B-C. There was no significant difference in the expression of NF-κB and STAT3 between LPS (si-TNF-α) group and LPS (NC) group, indicating that TNF-α interference had no effect on the expression of NF-κB and STAT3 in LPS-treated macrophages, and TNF-α could not regulate NF-κB and STAT3.

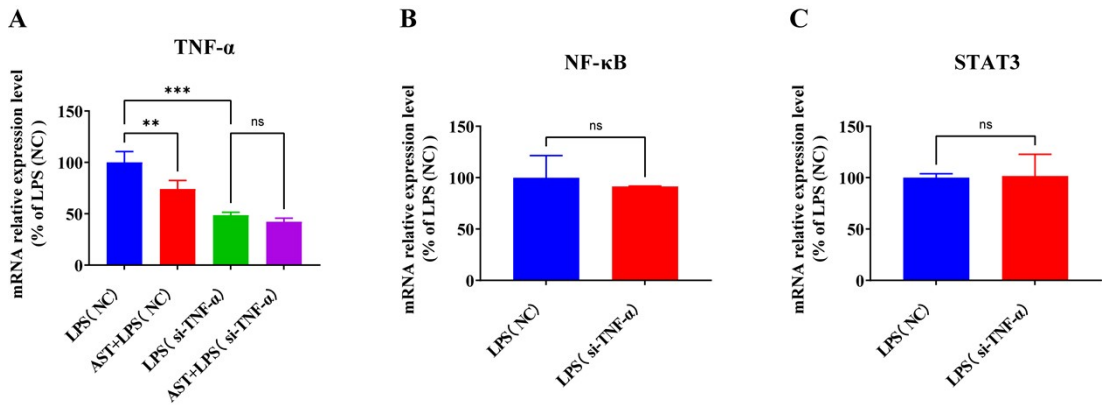

Fig. S5 The expression of TNF-α, NF-κB and STAT3 mRNA levels after the interference of TNF-α siRNA. (n = 3/group; mean ± SD; ** represent $p < 0.01$; *** represent $p < 0.001$; ns represent no significant difference compared with the control group.)

Table S1
PCR primer sequences.

Name	Sequence (5'→3')
H-pro-IL-1β-QF	ATGGACAAGCTGAGGAAGATG
H-pro-IL-1β-QR	CCCATGTGTCGAAGAAGATAGG

H-IL-1β-QF	CCTATTACAGTGGCAATGAGGATG
H-IL-1β-QR	AGTGGTGGTCGGAGATTCG
H-IL-6-QF	GAAAGCAGCAAAGAGGCACT
H-IL-6-QR	AGCTCTGGCTTGTTCCTCAC
H-IL-8-QF	CTGATTTCTGCAGCTCTGTG
H-IL-8-QR	GGGTGGAAAGGTTTGGAGTATG
H-TNF-α-QF	TGGGCAGGTCTACTTTGGGATCAT
H-TNF-α-QR	TTTGAGCCAGAAGAGGTTGAGGGT
H-NLRP3-QF	AACATGCCCAAGGAGGAAGA
H-NLRP3-QR	GGCTGTTCACCAATCCATGA
H-Caspase1-QF	GCACACGTCTTGCTCTCATT
H-Caspase1-QR	GCCTCCAGCTCTGTAGTCAT
H-COX-2-QF	CCAGCACTTCACGCATCAGT
H-COX-2-QR	ACGCTGTCTAGCCAGAGTTTCAC
H-NF-κB-QF	TGGGAATCCAGTGTGTGAAG
H-NF-κB-QR	CACAGCATTCAGGTCGTAGT
H-STAT3-QF	TCCATCAGCTCTACAGTGACAGC
H-STAT3-QR	TCCCAGGAGATTATGAAACACC
H-p53-QF	GCGTGTGGAGTATTTGGATGAC
H-p53-QR	AGTGTGATGATGGTGAGGATGG
H-β-Actin-QF	ATTGCCGACAGGATGCAGAA
H-β-Actin-QR	GCTGATCCACATCTGCTGGAA

Table S2
Partial core target attributes.
(The Degree value is used to screen the core targets and the target that is greater than the average Degree is considered as the core target)

Target	Betweenness Centrality	Closeness Centrality	Degree
IL6	0.303264191	0.85	84
TNF	0.272938466	0.836065574	82
MAPK3	0.07063399	0.653846154	52
PPARG	0.041104656	0.62195122	42
ESR1	0.015159691	0.573033708	34
MAPK1	0.009332702	0.566666667	34
MAPK14	0.011614205	0.566666667	34
PPARA	0.034632639	0.554347826	30
NR3C1	0.014905363	0.542553191	28
CYP19A1	0.006198011	0.542553191	26
PGR	0.010395156	0.53125	24
PTGES	0.063672786	0.536842105	24
AR	0.002258278	0.525773196	22
ALOX5	0.010923382	0.536842105	22
PTPN1	0.001227881	0.515151515	20
PTPN11	0.008488044	0.51	20
PTGER4	0.059099317	0.53125	20
PLA2G1B	0.012350352	0.525773196	20
PRKCA	0.002137623	0.515151515	20

Table S3
Binding energy of IL-6 and AST.

Ligand	Binding Energy	MMGBSA dG Bind (NS)
Astaxanthin	-11.1	-96.39
Control (Co-crystal)	-13.9	-68.13